Available online at www.sciencedirect.com
ScienceDirect
Clinical Biomechanics 22 (2007) 239–247
CLINICAL BIOMECHANICS
www.elsevier.com/locate/clinbiomech

Morphological muscle and joint parameters for musculoskeletal modelling of the lower extremity

M.D. Klein Horsman [a,*], H.F.J.M. Koopman [a], F.C.T. van der Helm [a], L. Poliacu Prosé [b], H.E.J. Veeger [c]

[a] *Institute for Biomedical Technology (BMTI), Biomedical Engineering Group, Department of Engineering Technology, University of Twente, P.O. Box 217, 7500 AE Enschede, The Netherlands*
[b] *Department of Anatomy, Vrije Universiteit, Amsterdam, The Netherlands*
[c] *Faculty of Human Movement Sciences, Vrije Universiteit, Amsterdam, The Netherlands*

Received 17 February 2006; accepted 3 October 2006

Abstract

Background. To assist in the treatment of gait disorders, an inverse and forward 3D musculoskeletal model of the lower extremity will be useful that allows to evaluate *if–then* scenarios. Currently available anatomical datasets do not comprise sufficiently accurate and complete information to construct such a model. The aim of this paper is to present a complete and consistent anatomical dataset, containing the orientations of joints (hip, knee, ankle and subtalar joints), muscle parameters (optimum length, physiological cross sectional area), and geometrical parameters (attachment sites, 'via' points).

Methods. One lower extremity, taken from a male embalmed specimen, was studied. Position and geometry were measured with a 3D-digitizer. Optotrak was used for measurement of rotation axes of joints. Sarcomere length was measured by laser diffraction.

Findings. A total of 38 muscles were measured. Each muscle was divided in different muscle lines of action based on muscle morphology. 14 Ligaments of the hip, knee and ankle were included.

Interpretation. The presented anatomical dataset embraces all necessary data for state of the art musculoskeletal modelling of the lower extremity. Implementation of these data into an (existing) model is likely to significantly improve the estimation of muscle forces and will thus make the use of the model as a clinical tool more feasible.
© 2006 Elsevier Ltd. All rights reserved.

Keywords: Lower extremity; Musculoskeletal model; Sarcomere length; Muscle parameters; Ligament

1. Introduction

Several musculoskeletal models have been developed to study for example gait, jumping or cycling (Zajac, 1989; Pandy, 2001). Most models reviewed by Pandy (2001) and Zajac (1989) are simple 2D models that can be used to gain insight in the principles of control of movement and the role of its components. To study the function of specific muscles for certain tasks more large scale musculoskeletal models are being used, for example to assist in the treatment of gait disorders by studying orthopaedic surgical procedures (Delp et al., 1990; Arnold et al., 2001). Arnold et al. (2001) estimated muscle tendon length of the hamstrings and psoas muscles of subjects with cerebral palsy, which is an important parameter in order to predict the biomechanical effect of a surgical intervention. Delp et al. (1990) studied the effect of a tendon transfer and lengthening by adjusting model parameters according to surgical techniques.

For studies focusing on the evaluation of specific, clinically relevant, questions, an accurate description of the

* Corresponding author.
E-mail address: m.d.kleinhorsman@utwente.nl (M.D. Klein Horsman).

0268-0033/$ - see front matter © 2006 Elsevier Ltd. All rights reserved.
doi:10.1016/j.clinbiomech.2006.10.003

geometry of the muscles and joints involved is important. The geometry of the musculoskeletal system defines the moment arms and the length of the muscles and thus the moment a muscle can generate at a joint given a muscle force. With this length of the musculotendon complex and geometric muscle parameters such as optimal fiber length, physiological cross sectional area (PCSA), the maximal muscle force can be estimated and used as a constraint in an optimisation to determine the actual muscle force for a specific movement or task.

To date, several anatomical studies have been published containing information on the modelling parameters for the lower extremity, containing for example muscle attachments sites (Pierrynowski, 1995; Brand and Crowinshield, 1982) or muscle parameters (Wickiewicz et al., 1983; Spoor et al., 1991; Weber, 1851). Unfortunately, none of these sets are complete, which implies that when constructing a complete musculoskeletal model different datasets have to be combined or missing parameters have to be estimated.

The study presented here is part of a larger project that aims to develop a model that allows clinicians to evaluate *if–then* scenarios with respect to treatment methods. For this a complete anatomical dataset will be necessary. Such a set should comprise data on joint properties, muscle actuation parameters and geometrical information, all from the same specimen.

2. Methods and results

Measurements were performed on a right lower extremity of a male embalmed specimen (age 77, height 1.74 m, weight 105 kg). Pre-experimental selection of the cadaver took place based on physical appearance. The specimen has a relatively high muscle mass and a high fat percentage for the upper body.

The cadaver was divided at the level of L1, so the attachment site of the psoas major could be measured. The specimen was fixed in a stainless steel frame, allowing easy positioning (Fig. 1). Four reference pins for measuring changes in orientation and position were placed in each of the body segment. The foot was defined as a system with three segments: hindfoot, midfoot and phalanges. These segments were constructed using k-wires. Due to the position during fixation the 'resting' position of the leg was with the hip externally rotated, the knee extended with the patella in the corresponding position and the foot in plantar flexion and supination.

Position was measured with a 3D-palpator (Pronk and Van Der Helm, 1991), which is a 3D-digitiser used for this type of measurements with a standard deviation of 1 mm per coordinate.

Although it falls outside the scope of this study, it is worth mentioning that prior to the dissection of the specimen, magnetic resonance images (MRI) were acquired for future evaluation of MRI-extracted parameters.

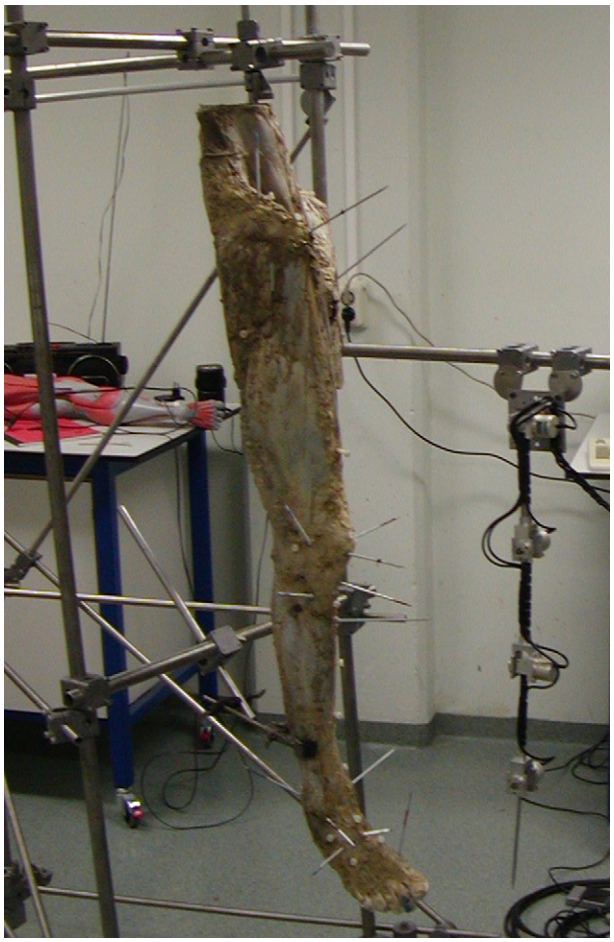

Fig. 1. Experimental setup with specimen fixed in frame.

2.1. Inertial parameters

Before dissection, anthropometric measurements (Clauser et al., 1969) were performed for estimation of inertial parameters. Segment mass and center of mass were calculated using regression equations of Clauser et al. (1969). Moments of inertia were calculated about the transversal and longitudinal axis of the segment (Yeadon and Morlock, 1989). See Table 1.

2.2. Palpable bony landmarks and reference pins

Prior to dissection 19 palpable bony landmarks were measured on the skin with the leg in the original fixated,

Table 1
Segment moments of inertia about the transversal (I_t) and longitudinal axis (I_l) in kg m^2, segment mass (kg) and center of mass with respect to the global frame with the leg in original fixated position (cm)

Segment	I_t	I_l	Mass	X	Y	Z
Pelvis	0.012	0.017	3.18	−1.76	5.45	5.42
Femur	0.197	0.058	11.54	6.45	−40.36	4.40
Tibia	0.058	0.007	4.00	6.46	−86.52	4.89
Foot	0.005	0.001	1.30	53.81	−84.75	5.11

or 'reference' position, together with the tips of the reference pins such that future local coordinate systems could be constructed. The choice of landmarks was based on the definition of local coordinate frames as described by the Standardization and Terminology Committee of the International Society of Biomechanics (Wu et al., 2002).

To facilitate interpretation, all data presented in this study were subsequently expressed in the coordinate frame of the pelvis (Fig. 2), with the hip center as origin and the axes defined as follows: (Wu et al., 2002)

Z: The line parallel to a line connecting the right and left anterior superior iliac spine (ASIS), pointing to the right.
X: The line parallel to a line lying in the plane defined by the two ASISs and the midpoint of the right and left posterior superior iliac spine (PSIS), orthogonal to the *Z*-axis, pointing anteriorly.
Y: The line perpendicular to *X* and *Z*, pointing cranially.

Table 2 gives the positions of the bony landmarks.

Since it was impossible to measure all anatomical structures without segmenting the leg, coordinates of the anatomical structures were always collected together with the tips of the reference pins in each session. These data were then rotated and translated to the 'reference' position, using the actual position of the reference pins and the position of these pins in the original position (Veldpaus et al., 1988). The error, as described by Veldpaus et al. (1988), is in the order of 1 mm per coordinate for each session.

2.3. Muscle and ligament attachment sites

To measure attachment sites, skin and subcutaneous fat were removed, even as the intra-muscular connections, resulting in muscles that were only connected to the bone at origin and insertion. The measuring procedure was as follows:

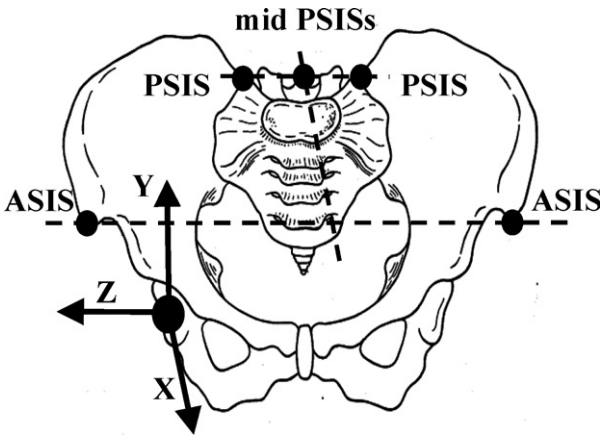

Fig. 2. Coordinate frame of the pelvis (*XYZ*) in which all data of this study were expressed as defined by Wu et al. (2002).

Table 2
Positions of bony landmarks with respect to the global frame with the leg in original fixated position (in cm)

Bony landmark	*X*	*Y*	*Z*
Pelvis			
Right anterior superior iliac spine	3.76	8.78	4.15
Left anterior superior iliac spine	3.76	8.78	−22.09
Right posterior superior iliac spine	−11.33	8.58	−4.53
Left posterior superior iliac spine	−11.14	8.97	−13.34
Right pubic tubercle	6.10	−0.02	−7.33
Left pubic tubercle	5.64	−0.05	−12.09
Femur			
Trochanter major	−5.98	−3.66	5.12
Medial femur epicondyle	7.68	−40.50	−3.21
Lateral femur epicondyle	3.17	−39.96	5.47
Tibia			
Medial tibia epicondyle	7.78	−44.05	−2.06
Lateral tibia epicondyle	3.28	−43.60	5.22
Tibial tuberosity	1.26	−45.65	5.21
Fibular head	8.74	−45.77	4.27
Medial malleolus	11.20	−79.21	1.04
Lateral malleolus	4.50	−81.59	4.55
Foot			
Navicular	10.51	−83.41	6.16
Proximal 1st metatarsal	14.71	−87.38	5.12
Proximal 5th metatarsal	9.96	−90.12	4.72
Distal 1st metatarsal (med)	19.82	−90.81	1.29
Distal 5th metatarsal (lat)	10.42	−95.04	4.52
Big toe (mid)	22.75	−94.83	6.83

(i) Careful removing of origin and insertion from bone.
(ii) Measurement of the attachment surface on the bone. In some cases a muscle was divided in different muscle parts based on differences in morphology.
(iii) Measurement of geometry of underlying tissue in case of intervening a straight muscle line of action.
(iv) Measurement of the position of the reference pins for expressing data in the 'reference' position.

In total 38 muscles were measured, divided in 57 muscle parts. Table 3[1] shows the measured muscles. The shape of the attachment sites of the muscle (parts) could be modelled as points, straight or curved lines or surfaces. To describe its mechanical effect accurately, the muscle element was divided in a sufficient number of muscle elements (Van Der Helm and Veenbaas, 1991) (see Table 3). The attachment site of the muscle (part) approximated by a point, was calculated as the mean of the measured coordinates on the bone. The error is defined as the mean distance of the measured coordinates to the calculated coordinate of the muscle element attachment site. Errors were in the order of 0.5 cm for most muscles. Two exceptions were found with errors up to 2.14 cm for the insertion of flexor and extensor digitorum longus, where 4 separate tendon slips attach to the different phalanges.

[1] Only a part of the data is presented here. The complete dataset is published on http://www.ctw.utwente.nl/staff/BW/M.D.KleinHorsman/.

Table 3
Per muscle part: origin, insertion described as surface, line (order) or point, divided in a number of elements and the muscle parameters: PCSA, optimal fiber length (L_{opt}), tendon length (L_{ten}), mass and pennation angle

Muscle	Origo	Ins.	# Elem.	S, BC or VP	PCSA (cm^2)	L_{opt} (cm)	L_{ten} (cm)	Mass (g)	Pen. ang. (°)
Add. brev. (prox.)	Surf.	Line (3)	6	S	3.8	9.5	0	38.3	0
Add. brev. (mid)				S	3.5	10.4	0	38.3	0
Add. brev. (dist)				S	3.2	11.2	0	38.3	0
Add. long.	Line (3)	Line (3)	6	S	15.1	10.6	0	168.5	0
Add. magn. (dist.)	Point	Line (2)	3	S	26.5	10.8	4.2	302.0	0
Add. magn. (mid.)	Surf.	Line (3)	6	S	22.1	10.4	0	243.0	0
Add. magn. (prox.)	Line (1)	Line (1)	4	S	5.0	10.7	0	56.0	0
Bic. fem. CL	Point	Point	1	S	27.2	8.5	13.0	245.0	30
Bic. fem. CB	Line (3)	Point	3	S	11.8	9.1	3.1	114.0	0
Ext. dig. long.	Line (2)	Point	3	VP	5.4	6.0	30.1	34.1	8
Ext. hal. long.	Line (2)	Point	3	VP	6.1	6.0	17.8	38.3	14
Flex. dig. long.	Surf.	Point	3	VP	6.6	3.8	16.6	26.7	28
Flex. hal. long.	Surf.	Point	3	VP	31.1	2.6	23.4	83.7	30
Gastrocn. (lat.)	Point	Point	1	BC	24.0	5.7	23.4	144.0	25
Gastrocn. (med.)	Point	Point	1	BC	43.8	6.0	21.2	278.0	11
Gemellus (inf.)	Point	Point	1	S	4.1	3.4	0	15.0	0
Gemellus (sup.)	Point	Point	1	S	4.1	3.4	0	15.0	0
Glut. max. (sup.)	Surf.	Surf.	6	S	49.7	12.0	0	629.0	0
Glut. max. (inf.)	Surf.	Line (2)	6	S	22.5	15.1	0	360.0	0
Glut. med. (ant.)	Surf.	Surf.	6	S	37.9	3.8	0	152.5	0
Glut. med. (post.)	Surf.	Surf.	6	S	60.8	4.5	3.0	287.0	16
Glut. min. (lat.)	Surf.	Point	3	S	10.0	2.8	7.3	29.1	0
Glut. min. (mid.)				S	8.1	3.4	7.3	29.1	0
Glut. min. (med.)				S	7.4	3.7	7.3	29.1	0
Gracilis	Line (1)	Point	2	VP	4.9	18.1	14.0	92.9	0
Iliacus (lat.)	Surf.	Point	3	BC	6.6	10.3	11.3	71.5	26
Iliacus (mid.)	Surf.	Point	3	BC	13.0	5.2	11.3	71.5	0
Iliacus (med.)	Surf.	Point	3	BC	7.6	8.9	15.5	71.5	0
Obt. ext. (inf.)	Line (1)	Point	2	S	5.5	6.9	3.5	40.0	0
Obt. ext. (sup.)	Surf.	Point	3	VP	24.6	2.8	3.0	72.0	0
Obturator int.	Surf.	Point	3	VP	25.4	2.1	8.2	55.0	0
Pectineus	Line (1)	Line (1)	4	S	6.8	11.5	0	82.4	0
Peroneus brev.	Surf.	Point	3	VP	19.0	2.7	6.4	53.9	23
Peroneus long.	Surf.	Point	3	VP	23.9	3.4	15.9	86.0	16
Peroneus tert.	Line (2).	Point	3	VP	6.2	4.3	10.0	28.0	19
Piriformis	Point	Point	1	S	8.1	3.9	1.6	33.0	0
Plantaris	Point	Point	1	S	2.4	4.8	35.0	12.0	0
Popliteus	Point	Line (1)	2	VP	10.7	2.4	1.0	27.0	0
Psoas minor	Point	Point	1	S	1.1	5.9	15.2	7.0	0
Psoas major	Surf.	Point	3	BC	19.5	9.9	11.3	204.0	13
Quadratus fem.	Line (1)	Line (1)	4	S	14.6	3.4	0	52.0	0
Rectus fem.	Point	Line (1)	2	S	28.9	7.8	9.6	239.0	22
Sartorius (prox.)	Point	Point	1	VP	5.9	34.7	7.9	217.0	0
Sartorius (dist.)	Point	Point	1	VP	5.9	34.7	7.9	217.0	0
Semimembr.	Point	Point	1	S	17.1	8.1	15.7	146.0	25
Semitend.	Point	Point	1	VP	14.7	14.2	23.7	220.0	0
Soleus (med.)	Line (2)	Point	3	S	94.3	2.4	8.5	238.5	64
Soleus (lat.)	Line (2)	Point	3	S	85.9	2.6	8.5	238.5	59
Tensor fasc. l.	Line (1)	Point	2	S	8.8	9.5	0	88.0	0
Tibialis ant.	Surf.	Point	3	VP	26.6	4.6	23.5	129.0	10
Tibialis post. (med.)	Surf.	Point	3	VP	21.6	2.4	11.0	55.9	25
Tibialis post. (lat.)	Surf.	Point	3	VP	21.6	2.4	11.0	55.9	43
Vastus interm.	Surf.	Line (1)	6	S	38.1	7.7	12.6	309.0	12
Vastus lat. (inf.)	Surf.	Line (2)	6	S	10.7	4.2	9.6	48.0	0
Vastus lat. (sup.)				S	59.0	9.1	9.6	568.0	0
Vastus med. (inf.)				S	9.8	7.6	9.6	78.0	0
Vastus med. (mid.)				S	23.2	7.6	9.6	186.0	0
Vastus med. (sup.)				S	26.9	8.3	9.6	236.0	0

A muscle line can be straight (S), curving around a bony contour (BC) or consist of via points (VP).

In case of a straight or curved line shaped attachment site, a 3D polynomial, parameterized for the *x*-, *y*- and *z*-coordinates was fitted to the measured coordinates. The resulting attachment sites of the muscle elements were pro-

Table 4
Origin and insertion of ligaments in cm with respect to the global frame with the leg in original fixated position

Ligament	Origin (cm)			Insertion (cm)		
	X	*Y*	*Z*	*X*	*Y*	*Z*
Iliofemoral lig. ant.	2.0	3.1	1.1	−2.2	−3.7	1.2
Iliofemoral lig. lat.	1.2	3.3	2.0	−2.2	−3.7	1.2
Pubofemoral lig.	2.7	−0.6	−3.6	−4.0	−1.4	4.1
Ischiofemoral lig.	−2.9	−1.3	0.0	−4.1	−0.4	0.9
Patellar lig.	10.2	−39.7	3.6	8.5	−45.5	3.8
Tibial collateral lig.	7.6	−39.6	−3.2	7.5	−48.4	0.1
Fibular collateral lig.	3.0	−40.3	5.0	1.2	−45.4	4.3
Anterior cruciate lig.	5.8	−41.2	−0.1	6.2	−41.8	0.9
Posterior cruciate lig.	4.4	−40.3	1.2	3.5	−43.3	0.2
Oblique popliteal lig.	3.3	−37.9	3.0	3.5	−44.0	−2.3
Posterior tibiotalar lig.	10.2	−80.1	0.4	8.2	−80.5	1.0
Tibiocalcaneal lig.	11.1	−79.8	1.0	9.6	−82.5	1.0
Tibionavicular lig.	11.7	−79.7	1.9	11.9	−83.6	3.5
Posterior talofibular lig.	6.8	−80.7	5.0	6.6	−81.0	2.0
Calacaneofibular lig.	5.9	−81.7	4.4	4.2	−83.5	1.3

portionally distributed along the polynomial. Based on (Van Der Helm and Veenbaas, 1991), for a first order polynomial at least 2 attachment sites and for a higher order polynomial at least 3 attachment sites were defined. The error of the 3D polynomial fit, defined as the mean distance of the data points to the polynomial, had a maximal value of 0.46 cm for the origin of the lateral part of the soleus.

For a surface attachment site, the measured coordinates were defined as a plane (Van Der Helm et al., 1992), where the measured coordinates were projected on that plane. The circumference of the projected coordinates could define an area, divided in 3 equal parts. For each part, 2 elements were proportionally distributed over the area resulting in 6 points describing the surface. For surface shaped attachment sites the error was defined as the mean distance of the measured coordinates to the optimized plane. It had a maximal value of 0.42 cm for the origin of the gluteus minimus.

The above process resulted in a total of 163 muscle elements for the 58 muscle parts as described in Table 3 and the *Web Supplementary Material*.

14 Ligaments of the hip, knee and ankle joint were measured (Table 4). Ligaments were considered as a straight line between origin and insertion.

2.4. Bony contours and via points

In case of a curvature of the muscle line of action due to underlying structures, two methods were used to describe this change in muscle force direction.

If a muscle line of action was intervened by the surface of an underlying bone and the muscle was free to shift over this surface, the resulting curved line of action was defined around this bony contour using a mathematical representation of this bone (Van Der Helm et al., 1992). In that case the surface was digitized and a geometric shape was fitted to the measured data points using an optimization described by Van Der Helm et al. (1992). This resulted in two relevant geometries (Table 5). Cylinder 1, representing the femur condyle, is meant to describe the curved line of action of the gastrocnemius around this structure. The second cylinder describes the curve of the iliopsoas around the pubis of the pelvis.

For 19 other muscle (parts) a curvature of the line of action was observed but a free shift of the muscle over the underlying structure was not possible, as in tibialis posterior, or in sartorius. In these cases 'via' points were defined, dividing the involved muscle in series of straight line segments (Delp et al., 1990). See *Web Supplementary Material*.

2.5. Axis and center of rotation

After removal of all muscles but with the ligaments still intact, the orientation of rotation axes and the position of the center of rotation of the hip, knee, ankle and subtalar joint were measured on the basis of the kinematic behaviour of these joints. Endo/exo rotation, flexion/extension, ab/adduction were manipulated by hand for each joint. The movement was limited by bone contact or ligaments. During these motions, segment motions were measured with Optotrak® (100 Hz, Nothern Digital Inc., Waterloo, Ontario, Canada). A cluster of 4 Optotrak markers was rigidly connected on the pelvis, femur, tibia and foot. For expression of these data in the 'reference' position, the positions of the reference pins were measured with a pointer. Instantaneous helical axis of the joints were determined from the position data of the marker clusters (Woltring, 1990; Veeger et al., 1997). Rotation centers and axes are described by respectively the pivot point and optimal direction vector (Woltring, 1990). The error e of the estimation of the rotation center and axis was calculated successively as (Veeger et al., 1997):

$$e_p = \frac{1}{N}\sum_{i=1}^{N} \mathrm{norm}(P_{\mathrm{opt}} - P_i) \tag{1a}$$

$$e_v = \frac{1}{N}\sum_{i=1}^{N} \arccos(V_{\mathrm{opt}} \cdot V'_i) \tag{1b}$$

Table 5
Bony contours

	sx	*sy*	*sz*	d*x*	d*y*	d*z*	*R*	*e* (cm)
Cylinder 1	6.06	−40.22	−1.75	−0.37	0.04	0.93	2.46	0.05
Cylinder 2	−1.27	0.97	−1.75	0.21	−0.14	−0.79	3.99	0.10

sx, *sy*, *sz* are coordinates (in cm) of an arbitrary point on the central axis with a direction [d*x* d*y* d*z*], expressed with respect to the global frame with the leg in original fixated position. *R* is the radius (in cm), *e* is the mean distance of the datapoints to the cylinder.

See Table 5 for the direction of the rotation axes and the position of the rotation centers with the corresponding error.

The movement of the patella could be approximated as a rotation of this segment with respect to the femur. For the determination of the rotation center and axis, 3 Optotrak markers were mounted on the patella in addition to the 4 markers on the femur. To account for the effect of the quadriceps muscles, an isometric spring was attached to the tendon of the quadriceps and the anterior superior iliac spine to keep the tendon under tension during knee flexion. The mean position of the 3 markers during knee flexion could be described with a circular shaped polynomial. These data points were fitted onto a plane and a circle was fitted on the resulting coordinates. The normal vector of the plane was then defined as the rotation axis and the center of the circle as the rotation center (Table 6). As can be seen these values differ from the knee axis and rotation center. The mean distance of the measured data points to the estimated plane was 0.09 cm. The mean distance to the circle was 0.02 cm.

After the separation of segments, a raster of evenly distributed points was measured on the surface of the femoral head and a sphere was fitted to the points on the articular surface. The position of the center of this sphere can be used as a second estimation of the rotation center of the hip joint. The mean distance e of a data point to the calculated sphere is defined as a measure for the accuracy of the optimization (Table 6).

2.6. Muscle parameters

The dissected muscles were weighed, after removing of the tendon, fat and excessive connective tissue, using a scale with an accuracy of 0.1 g. Belly, tendon and muscle fiber length were measured with the palpator, by calculating the distance between begin and end point. The length of at least five representative fibers was measured depending on the size of the muscle. Standard deviation (SD) in fiber length within a muscle was around 0.5 cm for most muscle parts as can be found in the *Web Supplementary Material*. Exceptions were measured in the gluteus maximus, extensor digitorum longus, add. magnus and gracilis muscle (SD up to 4.7 cm).

The pennation angle was determined using the palpator by calculating the angle of the direction at least five muscle fibers with the estimated line of action of the muscle. The vectors were defined by the difference between measured begin and end point. Pennation angles were measured in 20 of the 58 measured muscle parts. Standard deviations within the muscle parts were in the order of 4°. For the other muscle parts pennation angles were small and considered zero.

Sarcomere length, needed for determining optimal fiber length, was measured with a He–Ne laser (Young et al., 1990). By positioning a fiber in the 1 mm beam at a fixed distance from a scale, the diffraction pattern, representing the sarcomere length, can be read directly. Fibers were isolated using a microscope (magnitude 20×). The resolution was 0.05 μm depending on the quality of the embalmed fiber. In general from a muscle 6 samples of 6 fibers were measured depending on the size of the muscle. For the smaller muscles a minimum of 3 fibers were measured and for larger muscles like the m. vastus lateralis up to 10 fibers were isolated for diffraction.

The optimal fiber length of a muscle (part) was calculated as the mean of the actual muscle fibers length for a muscle multiplied by the ratio of the optimal sarcomere length of 2.7 μm (Walker and Schrodt, 1974) and the mean sarcomere lengths of the fibers of that muscle.

PCSA at optimal muscle length was defined as the muscle volume divided by the optimal fiber length, where muscle volume is defined as muscle mass divided by its density (1.056 g/cm^3 (Klein Breteler et al., 1999)). Largest PCSA (82.6 cm^2) was determined for the soleus muscle due to relatively small fiber length.

Tendon PCSA was determined by calculating the area of a circular, ellipsoid or rectangular assumed cross section using the measured width and breadth of a tendon area (see Web Supplementary Material).

Table 6
Estimated rotation centers (in cm) and rotation axes expressed in the global frame with the leg in original fixated position

Rotation center	*X*	*Y*	*Z*	*e* (cm)
Hip	0	0	0	0.02
Knee	3.84	−40.78	1.38	0.79
Femur-patella	3.51	−38.51	1.90	0.02
Ankle	9.33	−81.36	3.14	0.37
Subtalar	10.87	−80.61	3.36	0.37
Rotation axis	***X***	***Y***	***Z***	***e* (°)**
Knee	−0.528	−0.107	0.843	4.73
Femur-patella	−0.465	0.024	0.885	0.09 (cm)
Ankle	−0.730	−0.206	0.652	6.36
Subtalar	−0.780	−0.223	−0.584	8.63

Hip rotation center is based on a spherical fit through the surface of the femoral head. Knee, ankle and subtalar rotation axis and center with the corresponding error e (Eq. (1)) are based on instantaneous helical axis calculations as described by Veeger et al. (1997). The femur-patella joint is based on a circular fit through the trajectory of the patella with respect to the femur.

3. Discussion

This study generated a unique anatomical dataset comprising all necessary data for musculoskeletal modelling of the lower extremity. It contains attachment sites of all the muscles of the lower extremity and if necessary the muscle is split up in different muscle elements to describe the mechanical effect more accurate. For each element the important muscle parameters for the estimation of force generating properties are given such as optimal fiber length. Also the joint parameters of the hip, knee, ankle and subtalar joint are included. The expression of all geometrical parameters, in combination with the bony land-

marks in the same 'reference' frame allows for expression in other local coordinate frames.

The presented data form one consistent dataset, which is a major advantage. When different datasets are used to construct a model, scaling between datasets is necessary to correct for inter-individual anatomical variations. The effect of scaling however is uncertain and inaccuracies and inconsistencies are inevitable. The combined datasets result in an anatomical configuration that never existed. In that case (unknown) interactions between different anatomical parameters could get lost. The complete dataset presented in this study is based on one cadaver, which results in a consistent dataset.

Attachment sites were represented by a number of coordinates depending on size. For line and surface attachments the error was small (<0.46 cm). Attachment sites of relatively long tendons to the bone were represented by a point. Some of these attachment sites had relatively large errors, e.g. the insertion of the semimembranosus ($e = 0.81$ cm). Because these tendons cannot exert a moment to the bone (Van Der Helm and Veenbaas, 1991), a point attachment site was still seen as an acceptable representation, despite the relatively large error.

With the distance between its origin and insertion, the length of a ligament can be calculated in 'reference' position. The utilization of these data is limited in models that take stresses in ligaments into account. With the stress–strain relation of the ligament, the stress could be estimated given a certain initial stress and change of length. The calculated ligament lengths however contain small errors due to model assumptions that lead to very large errors in stresses. Secondly, the initial stress in the ligaments in the 'reference' position is unknown.

Several groups reported fiber lengths in muscles of the lower extremity (Yamaguchi et al., 1990). A few groups measured sarcomere length for a limited number (max. 27) of leg muscles to calculate optimal fibre length (Spoor et al., 1991; Wickiewicz et al., 1983). In this study we reported optimal fiber lengths for 58 muscle parts. The measured actual fiber length show small standard deviations within a muscle part. If larger variations occurred as in the iliacus, the muscle was split up in different parts. The optimal fiber length was based on sarcomere length measurements using laser diffraction, a very accurate method for measuring sarcomere lengths. Mean sarcomere lengths were found between 2 and 3.7 μm, which is a range consistent with the sliding filament theory according to Walker and Schrodt (1974). This makes it likely that filament length did not change as a result of the embalming process. This assumption is strengthened by the results of a study in rats in which the length change of muscle fibers in muscles fixed intact on the skeleton appeared to be negligible as a result of an embalming process (Cutts, 1988). The isolation of a fiber from a muscle part did not change the sarcomere length as observed in other studies (Klein Breteler et al., 1999). For a few samples no diffraction pattern was observed. It is assumed that this was caused by broken filaments due to embalming process or rigor mortis. These samples were considered as artefacts and were further ignored.

PCSA, calculated in this study as muscle volume divided by optimal fiber length, is an important parameter for the estimation of relative force distribution in musculoskeletal models. To have a good estimation of the relative muscle force, PCSA should be determined using one method and based on one cadaver. A comparison with other datasets based on different calculation methods and specimens is difficult. The exact calculation procedure however is less important than the use of a consistent dataset.

When pennation angles are compared to the datasets reviewed by Yamaguchi et al. (1990), there are 2 muscles that show large differences. The soleus muscle has angles up to 64° for the medial part in contrary to 32° measured by Friederich and Brand (1990). Wickiewicz et al. (1983) however reported areas in the soleus muscle up to 60°, which is comparable to our results. Yamaguchi only reports one pennation angle for the tibialis posterior, in this study a lateral part is defined as an extra element with larger angles (43°).

The accuracy of rotation centers and axes is crucial in terms of kinematics and kinetics. The hip joint is characterized as a ball-and socket joint and its rotation center can be estimated using a kinematic or geometric approach. Kinematic joint center and axes were constructed from motion data. A reconstruction of the hip joint rotation center by calculation of the optimal pivot point is shown in Fig. 3. The mean distance of each helical axis to the pivot point is 0.85 cm. A comparison with the geometric rotation center could not be made due to a missing reference point. However, as for the glenohumeral joint, it is very likely that both methods come up with comparable results (Veeger, 2000). When the geometric rotation center is compared with an estimated hip joint center based on regression

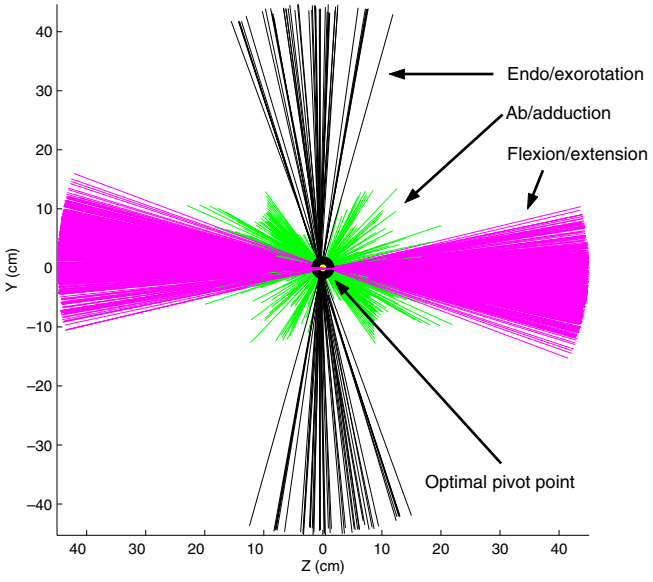

Fig. 3. Frontal view of hip rotation centre, defined as the optimal pivot point, calculated with instantaneous helical axes of recorded hip rotations around three anatomical axes.

equations using bony landmarks (Leardini et al., 1999; Bell et al., 1990), the calculated difference of 1.60 cm is within the range described by Leardini et al. (1999).

We considered the knee, ankle and subtalar joint in this study as a hinge with a fixed position and orientation. In reality these joint axes will alter during the arc of motion (e.g. (Lundberg et al., 1989) for the ankle joint) as can be seen in the error for the determination of the rotation axes. The error for the estimation of the rotation center of the knee was larger than the error for the ankle and subtalar axis. This was mainly caused by the translation of the knee rotation center due to rotation of the condyle of the femur over the tibia plateau. This movement of the femur condyle with respect to the tibia plateau is constrained by ligaments and menisci. This explained the difference in the axis of the cylinder fitted on the femur condyle and the optimal knee axis during a knee flexion (Tables 5 and 6). With a plane and circle fit, a rotation axis and center of the patella with respect to the femur can be estimated with a high accuracy. The calculation of instantaneous helical axes did not lead to accurate results because rotations round the longitudinal axis of the patella occurred. These rotations were due to the lack of the stabilizing effect of the surrounding muscles. By taking the mean position of the 3 markers, this irrelevant effect was not taken into account and only the translation in the sagittal plane was used. For musculoskeletal modelling the position of the attachment sites of the quadriceps on the patella is an important factor for calculation of the moment arm of these muscles during knee flexion. Rotations of the relatively small patella round its longitudinal axis will have small effects on the position of the attachment site. We believe that the position can be estimated sufficiently accurate with the used method.

The dataset in this study comprises the geometry of one, unique, individual. Scaling of data to a particular patient or subject to adapt the model to the anatomy of that subject has an uncertain effect. MRI can be used to collect subject specific parameters, but only to a limited extent. Recognition of attachment sites on the bone and fiber orientation is still difficult in MR images, which makes the calculation of muscle lines of action arbitrary, at least. In addition, MRI data can at this point only produce geometry data, while important parameters for muscle force estimation such as optimal fiber length will still be based on cadaver data.

The development of subject specific models comprising all the anatomic parameters of the subject will be one of the future challenges in musculoskeletal modelling, but this might still be a long way to go. In the meantime modelling data as presented in this study will be of great value.

Appendix A. Supplementary data

Supplementary data associated with this article can be found, in the online version, at doi:10.1016/j.clinbiomech.2006.10.003.

References

Arnold, A.S., Blemker, S.S., Delp, S.L., 2001. Evaluation of a deformable musculoskeletal model for estimating muscle-tendon lengths during crouch gait. Ann. Biomed. Eng. 29, 263–274.

Bell, A.L., Pedersen, D.R., Brand, R.A., 1990. A comparison of the accuracy of several hip center location prediction methods. J. Biomech. 23, 617–621.

Brand, R.A., Crowinshield, R.D., 1982. A model of lower extremity muscular anatomy. J. Biomech. 104, 153–161.

Clauser, C.E., Mcconville, J.T., Young, J.M., 1969. Weight, volume and center of mass of segments of the human body. Wright-Patterson Air Force Base Ohio (AMRL-TR-69-70), pp. 339–356.

Cutts, A., 1988. Shrinkage of muscle fibres during the fixation of cadaveric tissue. J. Anat. 160, 75–78.

Delp, S.L., Loan, J.P., Hoy, M.G., Zajac, F.E., Topp, E.L., Rosen, J.M., 1990. An interactive graphics-based model of the lower extremity to study orthopaedic surgical procedures. IEEE Trans. Biomed. Eng. 37, 757–767.

Friederich, J.A., Brand, R.A., 1990. Muscle fiber architecture in the human lower limb. J. Biomech. 23, 91–95.

Klein Breteler, M.D., Spoor, C.W., Van Der Helm, F.C., 1999. Measuring muscle and joint geometry parameters of a shoulder for modeling purposes. J. Biomech. 32, 1191–1197.

Leardini, A., Cappozzo, A., Catani, F., Toksvig-Larsen, S., Petitto, A., Sforza, V., Cassanelli, G., Giannini, S., 1999. Validation of a functional method for the estimation of hip joint centre location. J. Biomech. 32, 99–103.

Lundberg, A., Svensson, O.K., Nemeth, G., Selvik, G., 1989. The axis of rotation of the ankle joint. J. Bone Joint Surg. Br. 71, 94–99.

Pandy, M.G., 2001. Computer modeling and simulation of human movement. Annu. Rev. Biom. Eng. 3, 245–273.

Pierrynowski, M.R., 1995. Analytic representation of muscle line of action and geometry, In: Allard, P., Stokes, I.A.F. & Blanchi, J.P. (Eds.), Three-Dimensional Analysis of Human Movement. Human Kinetics, Champaign, IL, pp. 214–256.

Pronk, G.M., Van Der Helm, F.C., 1991. The palpator: an instrument for measuring the positions of bones in three dimensions. J. Med. Eng. Technol. 15, 15–20.

Spoor, C.W., Van Leeuwen, J.L., Van Der Meulen, W.J., Huson, A., 1991. Active force-length relationship of human lower-leg muscles estimated from morphological data: a comparison of geometric muscle models. Eur. J. Morphol. 29, 137–160.

Van Der Helm, F.C., Veeger, H.E., Pronk, G.M., Van Der Woude, L.H., Rozendal, R.H., 1992. Geometry parameters for musculoskeletal modelling of the shoulder system. J. Biomech. 25, 129–144.

Van Der Helm, F.C., Veenbaas, R., 1991. Modelling the mechanical effect of muscles with large attachment sites: application to the shoulder mechanism. J. Biomech. 24, 1151–1163.

Veeger, H.E., 2000. The position of the rotation center of the glenohumeral joint. J. Biomech. 33, 1711–1715.

Veeger, H.E., Yu, B., An, K.N., Rozendal, R.H., 1997. Parameters for modeling the upper extremity. J. Biomech. 30, 647–652.

Veldpaus, F.E., Woltring, H.J., Dortmans, L.J., 1988. A least-squares algorithm for the equiform transformation from spatial marker co-ordinates. J. Biomech. 21, 45–54.

Walker, S.M., Schrodt, G.R., 1974. I segments lenghts and thin filament periods in skeletal muscle fibers of the rhesus monkey and the human. Anat. Rec. 178, 63–82.

Weber, E., 1851. Über die langenverhaltnisse der fleischfasern der muskeln im algemeinen. Berichte u. d. Verh. d. Konigl. Sachs. Ges. d. Wiss. Math.-Phys. CL., pp. 5–86.

Wickiewicz, T.L., Roy, R.R., Powell, P.L., Edgerton, V.R., 1983. Muscle architecture of the human lower limb. Clin. Orthop., 75–83.

Woltring, H.J., 1990. Estimation of the trajectory of the instantaneous centre of rotation in planar biokinematics. J. Biomech. 23, 1273–1274.

Wu, G., Siegler, S., Allard, P., Kirtley, C., Leardini, A., Rosenbaum, D., Whittle, M., D'lima, D.D., Cristofolini, L., Witte, H., Schmid, O., Stokes, I., 2002. ISB recommendation on definitions of joint coordinate system of various joints for the reporting of human joint motion–part I: ankle, hip, and spine. International society of biomechanics. J. Biomech. 35, 543–548.

Yamaguchi, G.T., Sawa, A.G.U., Moran, D.W., Fessler, M.J., Winters, J.M., 1990. A survey of human musculotendon actuator parameters. In: Winter, J.M., Woo, S.L.Y. (Eds.), Multiple Muscle Systems: Biomechanics and Movement Organisation. Springer, Berlin, pp. 717–773.

Yeadon, M.R., Morlock, M., 1989. The appropriate use of regression equations for the estimation of segmental inertia parameters. J. Biomech. 22, 683–689.

Young, L.L., Papa, C.M., Lyon, C.E., George, S.M., Miller, M.F., 1990. Comparison of microscopic and laser diffraction methods for measuring sarcomere lengths of contracted muscle fibers of chicken pectoralis major muscle. Poult. Sci. 69, 1800–1802.

Zajac, F.E., 1989. Muscle and tendon: properties, models, scaling, and application to biomechanics and motor control. Crit. Rev. Biomed. Eng. 17, 359–411.